Comparison of coherence times in three dc SQUID phase qubits

Hanhee Paik, B. K. Cooper, S. K. Dutta, R. M. Lewis, R. C. Ramos, T. A. Palomaki, A. J. Przybysz, A. J. Dragt, J. R. Anderson, C. J. Lobb, and F. C. Wellstood

***Abstract*— We report measurements of spectroscopic linewidth and Rabi oscillations in three thin-film dc SQUID phase qubits. One device had a 6-turn Nb loop, the second had a single-turn Al loop, and the third was a first order gradiometer formed from 6-turn wound and counter-wound Nb coils to provide isolation from spatially uniform flux noise. In the 6 - 7.2 GHz range, the spectroscopic coherence times for the gradiometer varied from 4 ns to 8 ns, about the same as for the other devices (4 to 10 ns). The time constant for decay of Rabi oscillations was significantly longer in the single-turn Al device (20 to 30 ns) than either of the Nb devices (10 to 15 ns). These results imply that spatially uniform flux noise is not the main source of decoherence or inhomogenous broadening in these devices.**

***Index Terms*— qubit, decoherence, flux noise, Rabi oscillation**

I. Introduction

DESPITE much recent progress in the use of superconducting devices for quantum computation [1], decoherence still presents a major challenge. For Josephson phase qubits [2]–[8], Martinis *et al.* [9] have proposed that dielectric loss and two-level fluctuators in dielectrics are the primary cause of decoherence. They showed significant improvement could be obtained by replacing lossy dielectrics with lower-loss materials. Van Harlingen *et al.* [10] argued that while critical current fluctuations would produce decoherence, the observed coherence times in flux and phase qubits were much shorter than would be expected from the level of critical current noise that has been typically observed in tunnel junctions [11]–[13]. Similarly, Martinis *et al.* [14] have argued that charge noise should have a small impact on the coherence time of phase qubits due to their large junction capacitance. Recently, Bertet *et al.* reported that decoherence in their flux qubit came from the detection dc SQUID [15].

Flux noise is another possible source of decoherence in phase qubits as most are essentially rf or dc SQUIDs. In this paper, we compare Rabi oscillations and spectroscopic coherence times in three dc SQUID phase qubits that were built with a single-turn magnetometer configuration (AL1), a multi-turn magnetometer configuration (NB1) and a gradiometer configuration (NBG) respectively. Although we did not perform a direct test on the gradiometer balance, the counter-wound configuration should make it much less sensitive to spatially unform magnetic fields than either of the magnetometers.

Manuscript received August 30, 2006. This work was supported by NSF under the Qubic program, the Laboratory for Physical Sciences, College Park, MD, and the Center for Superconductivity Research at the University of Maryland, College Park, MD 20742 USA. Hanhee Paik, B. K. Cooper, S. K. Dutta, R. M. Lewis, R. C. Ramos, T. A. Palomaki, A. J. Przybysz, A. J. Dragt, J. R. Anderson, C. J. Lobb, and F. C. Wellstood are with the the University of Maryland, College Park, MD 20742 USA. Corresponding author email: hanhee@umd.edu

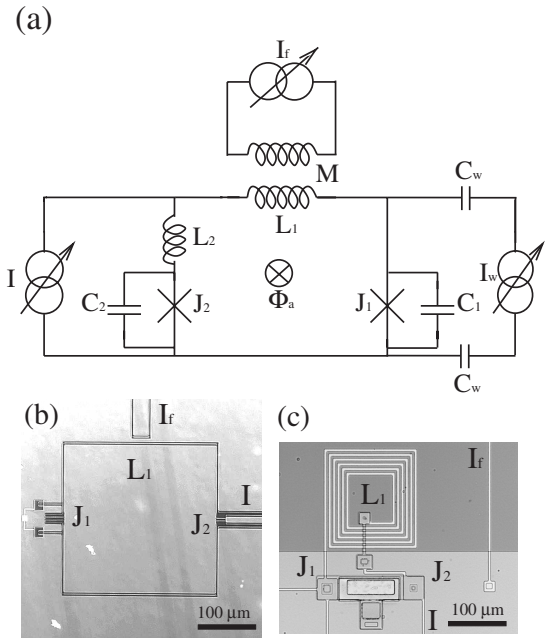

Fig. 1. (a) Schematic of dc SQUID phase qubit. I is the current bias, I_f is current for the flux bias, M is mutual inductance between the flux bias coil and the SQUID loop and Φ_a is the applied flux in the SQUID loop. C_1 and C_2 are the capacitances of the qubit junction J_1 and the isolation junction J_2, respectively. Microwave source I_w is coupled to J_1 through capacitors C_w. Photographs of (b) Al single-turn SQUID magnetometer AL1 and (c) Nb 6-turn SQUID magnetometer NB1.

II. dc SQUID phase qubits without and with gradiometer loops

Figure 1(a) shows a schematic of a dc SQUID phase qubit [3]. We refer to J_1 as the qubit junction and J_2 as the isolation junction. In this qubit design, junction J_2 is needed to read out the state of J_1 via tunneling to the voltage state [3]. J_2 and inductor L_1 also inductively isolate the qubit from current noise on the bias leads. By choosing $L_1 \gg L_2 + L_{j2}$, where L_{j2} is the Josephson inductance of the isolation junction, current noise will be mainly diverted through J_2 rather than the qubit junction J_1.

Figures 1(b) and 1(c) show two of our SQUID phase qubits that have magnetometer loops. Device NB1 [see Fig. 1(b)] is

TABLE I

PARAMETERS FOR SQUIDS NBG, NB1 AND AL1. I_{01} AND I_{02} ARE THE CRITICAL CURRENTS OF J_1 AND J_2, RESPECTIVELY. $L_{j1}(0)$ AND $L_{j2}(0)$ ARE THE JOSEPHSON INDUCTANCES OF J_1 AND J_2 WHEN THEY ARE UNBIASED AND $\beta = (I_{01} + I_{02})L/\Phi_0$, WHERE L = L_1 + L_2 IS THE TOTAL INDUCTANCE OF THE SQUID LOOP.

Parameters	gradiometer NBG	magnetometer NB1	magnetometer AL1
I_{01} (μA)	23.0	33.8	21.275
I_{02} (μA)	3.8	4.8	9.445
C_1 (pF)	4.1	4.4	4.1
C_2 (pF)	2.0	2.2	2.1
$L_{j1}(0)$ (pH)	13.9	9.7	13.2
$L_{j2}(0)$ (pH)	84.9	68	44.5
L_1 (pH)	4540	3530	1236
L_2 (pH)	12	20	5
β	34	66	19

a thin-film Nb magnetometer with a 6-turn loop. The device was made at Hypres, Inc., from a $Nb/AlO_x/Nb$ trilayer using their 100 A/cm^2 process. The qubit junction has an area of 100 μm^2 and we applied a small magnetic field in the plane of the junctions to reduce the critical current of the device to the 10 to 30 μA range. Subsequent measurements on similar devices, which were not suppressed by magnetic field, yielded similar spectroscopic coherence times and Rabi decay times [17].

Device ALl is a single-turn dc SQUID magnetometer made from thin-film Al [see Fig. 1(c)]. We used photolithography and double-angle evaporation to form the loop and the $Al/AlO_x/Al$ tunnel junctions. The qubit junction has an area of the 80 μm^2. Other than AlO_x, no insulation layers were deposited on this device.

Device NBG (see Fig. 2) was made at Hypres from a $Nb/AlO_x/Nb$ trilayer using their 30 A/cm^2 process. The qubit junction has an area of 102 μm^2. The SQUID has two 6-turn thin-film Nb coils wound in opposition to form a magnetic field gradiometer. To apply a net flux to the device, we placed a flux bias line on the right side of the device (closer to coil L_{1a} than to L_{1b} in Fig. 2). All three devices were made on silicon wafers with a layer of thermally grown silicon dioxide.

III. EXPERIMENTAL SETUP

Device NB1 was measured on an Oxford Instruments Kelvinox model 200 dilution refrigerator at a base temperature of 25 mK, while devices AL1 and NBG were measured on an Oxford Instruments model 25 dilution refrigerator at a base temperature of 80 to 100 mK. Each device was mounted in a closed superconducting aluminum box to shield out magnetic fields. In addition, each refrigerator was surrounded by a room-temperature mu-metal shield and enclosed in an rf-shielded room. To characterize the devices, we measured the switching current as a function of the applied flux. By fitting the characteristics to those of an ideal dc SQUID we obtained the device parameters, summarized in Table 1.

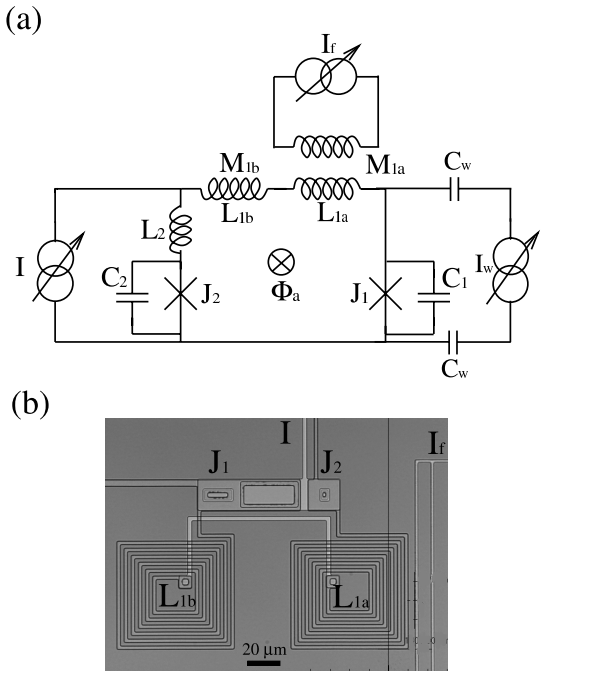

Fig. 2. (a) Schematic of dc SQUID phase qubit with a gradiometer. I is the current bias, I_f is current for the flux bias, Φ_a is the applied flux in the SQUID loop. C_1 and C_2 are the capacitances of junctions J_1 and J_2. L_{1a} and L_{1b} are inductances of each coil of the gradiometer, M_{1a} and M_{1b} are mutual inductances between each coil, respectively, and the flux bias line. A microwave source I_w is coupled to J_1 through capacitors C_w. (b) Photo of dc SQUID phase qubit, gradiometer NBG.

IV. MEASUREMENT OF ENERGY LEVELS

Before making any measurements on a SQUID, we use a flux shaking technique to initialize the flux state [16]. We then apply a simultaneous flux and current ramp so as to bias the qubit junction with current, and not the isolation junction. With this biasing scheme, our device acts as an ideal phase qubit with the two lowest levels in a well of the tilted washboard potential forming the qubit states, $|0\rangle$ and $|1\rangle$.

The qubit state can be monitored by measuring the rate at which the system tunnels to the voltage state [3]; the first excited state $|1\rangle$ typically tunnels about 500 times faster than the ground state $|0\rangle$. During the simultaneous current and flux ramp, we record the time at which the device escapes to the voltage state. We repeat this process on the order of 10^5 times to build up a histogram of escape events versus ramp time, which we convert to escape rate versus current (for spectroscopy) or escape rate versus time (for Rabi oscillations).

As an example, Fig. 3 shows the total escape rate of the qubit junction in device NBG as a function of the bias current I, with and without application of 6.6 GHz microwaves. Sweeping current through the qubit changes the energy level spacing adiabatically. When the microwaves comes into resonance with the energy level spacing, transitions to the excited state occur and we see enhancement in the total escape rate. In Fig 3, two clear resonance peaks are visible, at around 21.57

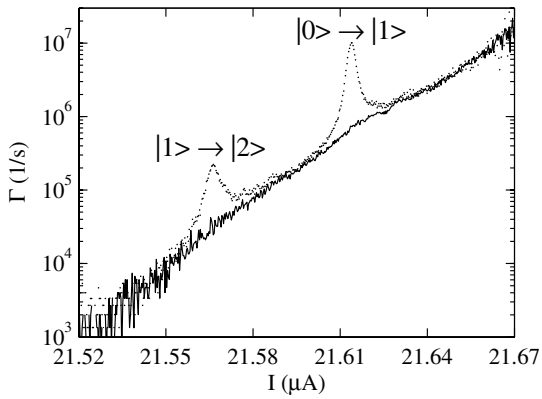

Fig. 3. Total escape rate vs. current for NBG at 100 mK. Dotted line is when 6.6 GHz microwave is applied to the qubit junction and solid line is without microwaves.

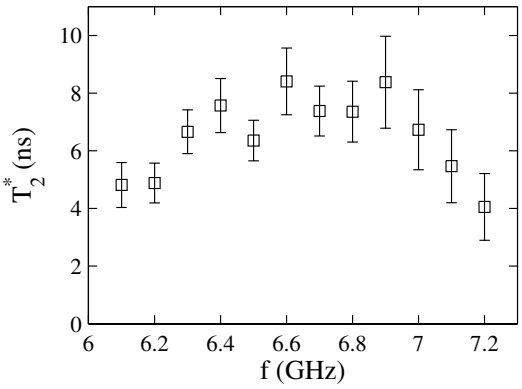

Fig. 4. Spectroscopic coherence time T_2^* of the $|0\rangle$ to $|1\rangle$ transition versus frequency for SQUID gradiometer NBG measured at 100 mK.

μA and 21.62 μA, corresponding to $|1\rangle \rightarrow |2\rangle$ and $|0\rangle \rightarrow |1\rangle$ transitions.

V. Measurement of T_2^*

To determine the spectroscopic coherence time T_2^* [18] of the $|0\rangle \rightarrow |1\rangle$ transition frequency f_{01}, we obtained the low-power half-width at half-maximum ΔI of the resonance peak and recorded its location $I(f_{01})$. Repeating this procedure for a range of applied microwave frequencies yields f_{01} and ΔI as a function of the ramp current I. The spectroscopic coherence time as a function of the frequency was then found from [18]

$$T_2^* = \frac{1}{2\pi \Delta I \frac{\partial f_{01}}{\partial I}}. \quad (1)$$

Figure 4 shows a plot of T_2^* versus microwave frequency for gradiometer NBG, measured at 100 mK. For frequencies in the 6.0 - 7.2 GHz range, T_2^* varied between about 4 ns and 8 ns. Spectroscopic measurements on magnetometers NB1 and AL1 revealed comparable variations in T_2^*, from about 4 to 10 ns in the same frequency range [17]. Since T_2^* is sensitive to low-frequency noise (inhomogenous broadening), as well as pure dephasing and dissipation [18], we can conclude that the combined effect of low-frequency noise, pure dephasing and dissipation is comparable in the three devices.

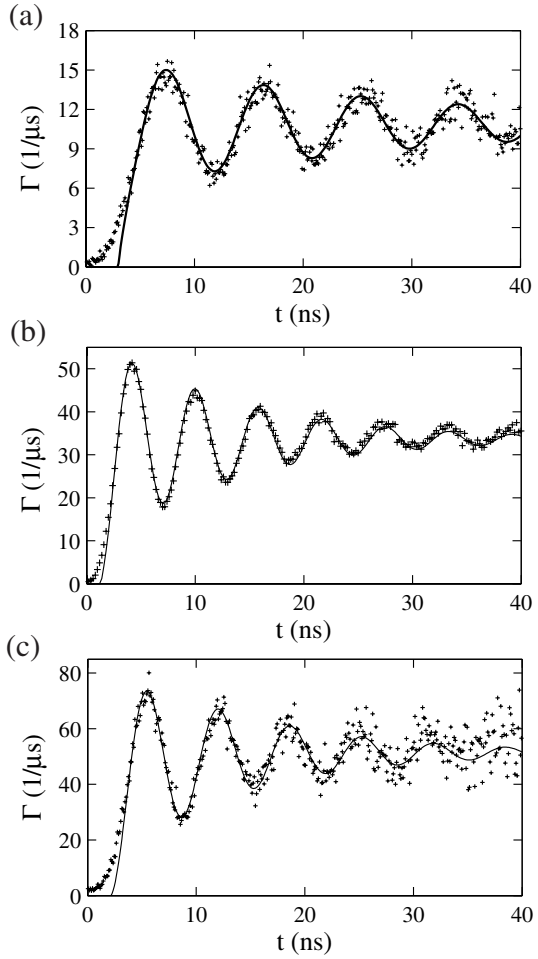

Fig. 5. Measurements of Rabi oscillation in the escape rate in (a) single-turn magnetometer AL1, (b) 6-turn magnetometer NB1, (c) gradiometer NBG. In each case the solid curve is a least-square fit to a cosine function with an exponential decay envelope.

VI. Comparisons of Rabi oscillations between a gradiometer and magnetometers

To distinguish the effects of low-frequency noise from dephasing processes, we also measured Rabi oscillations. The idea is that the envelope decay time constant T' of a Rabi oscillation is sensitive to noise at the Rabi frequency while the main effect of noise at much lower frequencies (which acts like inhomogenous broadening) is to change the shape of the envelope [10], [14]. This relative insensitivity of the Rabi oscillation to low-frequency noise is similar to the situation in a spin-echo measurement [14]. The envelope decay time constant T', the energy relaxation time T_1, and the coherence time T_2 are related by [19]

$$\frac{1}{T'} = \frac{1}{2T_1} + \frac{1}{2T_2}, \quad (2)$$

when the Rabi oscillation is driven on resonance. Although spin-echo measurements are the best way to directly determine T_2 and distinguish pure dephasing from inhomogenous broadening, we were not able to measure spin echoes in these devices due to their relatively short coherence times. Finally, from seperate measurements, we find T_1 is roughly 50 ns.

TABLE II
SUMMARY OF SPECTROSCOPIC COHERENCE TIME T_2^* AND TIME CONSTANT T' FOR DECAY OF RABI OSCILLATION.

	gradiometer NBG	magnetometer NB1	magnetometer AL1
T'(ns)	10 - 15	10 - 15	20 - 30
T_2^*(ns)	4 - 8	4 - 10	4 - 10

Figure 4 shows typical examples of measured Rabi oscillations in the total escape rate for the three devices. We applied microwave frequencies of 7.6 GHz for NB1 at 25 mK [see Fig. 4(a)], 7 GHz for AL1 at 80 mK [see Fig. 4(b)] and 6.5 GHz for NBG at 100 mK [see Fig. 4(c)]. The applied microwaves coupled to the qubit junction via a small capacitor [See Fig. 1 and Fig. 2] and resonantly drove the qubit between $|0\rangle$ and $|1\rangle$. In each case, we observed clear oscillations in the escape rate. In these plots, t = 0 indicates when the microwaves were turned on.

The solid curves in Fig. 4 are least-square fits to a cosine function with an exponential envelope with time constant T'. From the fits, T' for the gradiometer NBG was about 12 ns, while for magnetometers NB1 and AL2 it was about 12 ns and 27 ns, respectively (see Table 2). Density matrix simulations reveal that the escape rate we observe is dominated by a small population in $|2\rangle$ that escapes very rapidly ($\Gamma_2 \sim 10^{10}$ 1/s $\gg 1/T'$), and this population is directly proportional to the occupancy of $|1\rangle$ which escapes much more slowly ($\Gamma_1 \sim 10^7$ 1/s). While tunneling contributes to spectroscopic broadening [18], measurements over a wide range of conditions with different escape rates did not alter T' for Rabi oscillations in the total escape rate [17].

Thus the single-turn aluminum magnetometer AL1 had a substantially longer envelope decay time T' than either the Nb magnetometer or the Nb gradiometer. From this comparison, we can safely conclude that T' in our dc SQUID phase qubits is not being limited by spatially uniform flux noise. Finally, we note that since $T' \sim 2T_2^*$ (see Table 2), low-frequency noise is not causing significant inhomogeneous broadening of the resonance.

VII. CONCLUSION

In conclusion, we have measured the spectroscopic coherence time T_2^* and Rabi oscillations in three dc SQUID phase qubits. One device was a Nb gradiometer with 6-turn wound and counter-wound coils, the second was an Al magnetometer made with a single-turn loop, and the third was a Nb magnetometer with a 6-turn coil. The gradiometer did not show significantly longer T' or T_2^*, and in fact the single-turn Al magnetometer showed a significantly longer T' than either the Nb gradiometer or Nb magnetometer. We conclude that spatially uniform flux noise is not a dominant source of decoherence in our phase qubits. We cannot rule out the possibility of a local source of flux noise, which would not be nulled by a gradiometer.

ACKNOWLEDGMENT

The authors would like to thank M. Mandelberg, M. Manheimer, B. Palmer and F. W. Strauch for useful discussions.

REFERENCES

[1] J. Q. You, and Franco Nori, "Superconducting Circuits and Quantum Information", *Phys. Today*, vol. 58, No. 11, pp. 42 - 47, Nov. 2005.
[2] S. Han, Y. Yu, X. Chu, S.-I Chu, and Z. Wang, "Time-Resolved Measurement of Dissipation-Induced Decoherence in a Josephson Junction", *Science*, vol. 293, pp. 1457 - 1459, Aug. 2001.
[3] J. M. Martinis *et al.*, "Rabi Oscillations in a Large Josephson-Junction Qubit", *Phys. Rev. Lett.*, vol. 89, pp. 117901-1 - 117901-4, Sep. 2002.
[4] A. J. Berkley, *at al.*, "Entangled Macroscopic Quantum States in Two Superconducting Qubits", *Science*, vol. 300, pp. 1548 - 1550, Jun. 2003.
[5] S. K. Dutta, *et al.*, "Determination of Relaxation Time of a Josephson Junction Qubit", *Phys. Rev. B.*, vol. 70, pp. 140502(R)-1 - 140502(R)-4, Oct. 2004.
[6] J. Claudon, F. Balestro, F. W. J. Hekking, and O. Buisson, "Coherent Oscillations in a Superconducting Multilevel Quantum System", *Phys. Rev. Lett.*, vol. 93, pp. 187003-1 - 187003-4, Oct. 2004.
[7] K. B. Cooper, *et al.* "Observation of Quantum Oscillations Between a Josephson Phase Qubit and a Microscopic Resonator Using Fast Readout", *Phys. Rev. Lett.*, vol. 93, pp. 180401-1 - 180401-4, Oct. 2004.
[8] R. McDermott, *et al.*, "Simultaneous State Measurement of Coupled Josephson Phase Qubits", *Science*, vol. 307, pp. 1299 - 1302, Feb. 2005.
[9] J. M. Martinis *et al.*, "Decoherence in Josephson Qubits from Dielectric Loss", *Phys. Rev. Lett.*, vol. 95, pp. 210503-1 - 210503-4, Nov. 2005.
[10] D. J. Van Harlingen, *et al.*, "Decoherence in Josephson-Junction Qubits Due to Critical Current Fluctuations", *Phys. Rev. B.*, vol. 70, pp. 064517-1 - 064517-13, Aug. 2004.
[11] B. Savo, F. C. Wellstood, and J. Clarke, "Low-frequency Excess Noise in Nb-Al2O3-Nb Josephson Tunnel Junctions", *Appl. Phys. Lett.*, vol. 50, pp. 1757-1759, Jun. 1987.
[12] R. T. Wakai and D. J. Van Harlingen, "Direct Lifetime Measurements and Interactions of Charged Defect States in Submicron Josephson Junctions", *Phys. Rev. Lett.*, vol. 58, pp. 1687-1690, Apr. 1987.
[13] F. C. Wellstood, C. Urbina, and John Clarke, "Flicker (1/f) Noise in the Critical Current of Josephson Junctions at 0.09-4.2 K", *Appl. Phys. Lett.*, vol. 85, pp. 5296-5298, Nov. 2004.
[14] J. M. Martinis *et al.*, "Decoherence of a Superconducting Qubit Due to Bias Noise", *Phys. Rev. B*, vol. 67, pp. 094510-1 - 094510-10, Mar. 2003.
[15] P. Bertet, *et al.*,"Dephasing of a Superconducting Qubit Induced by Photon Noise", *Phys. Rev. Lett.*, vol. 95, pp. 257002-1 - 257002-4, Dec. 2005.
[16] T. A. Palomaki *et al.*, "Initializing the Flux State of Multiwell Inductively Isolated Josephson Junction qubits", *Phys. Rev. B*, vol. 73, pp. 014520-1 - 014520-7, Jan. 2006.
[17] S. K. Dutta, "Characterization of Josephson Devices For Use In Quantum Computation", Ph.D. thesis, University of Maryland, 2006.
[18] H. Xu *et al.*, "Spectroscopic Resonance Broadening in a Josephson Junction qubit Due to Current noise", *Phys. Rev. B*, vol. 71, pp. 064512-1 - 064512-11, Feb. 2005.
[19] H. C. Torrey, "Transient Nutation in Nuclear Magnetic Resonance", *Phys. Rev.*, vol. 76, pp. 1059 - 1068, Oct. 1949.